

# Swelling-induced modulation of static and dynamic fluctuations in polyacrylamide gels observed by scanning microscopic light scattering

Hidemitsu Furukawa\* and Kazuyuki Horie

*Department of Organic and Polymer Materials Chemistry, Tokyo University of Agriculture and Technology,  
2-24-16 Naka-cho, Koganei-shi, Tokyo 184-8588, Japan*

Ryunosuke Nozaki

*Department of Polymer Chemistry, Tokyo Institute of Technology, 2-1-1 O-okayama, Meguro-ku, Tokyo 152-8552, Japan*

Mamoru Okada

*1-6-3 Unoki, Ota-ku, Tokyo 146-0091, Japan*

(Received 7 April 2003; revised manuscript received 24 July 2003; published 22 September 2003)

The nature of inhomogeneities in vinylpolymer gels has hardly been clarified yet. Inhomogeneities on submicron and nanometer scales in polyacrylamide gels have been investigated by using a scanning microscopic light-scattering system and applying a general formula for an ensemble-averaged correlation function. The network structure of the gels is modified by varying the preparation conditions and can be roughly divided into two types. Swelling-induced modulation of inhomogeneities depends on the type of the network structure. At low monomer concentrations in preparation, both submicron- and nanometer-scale inhomogeneities increase with swelling. At high monomer concentrations in preparation, submicron-scale inhomogeneities increase with swelling, but nanometer-scale inhomogeneities decrease anomalously. This behavior is explained by a model of inhomogeneous network structure of vinylpolymer gels, where macrogel is formed from a large number of microgel particles.

DOI: 10.1103/PhysRevE.68.031406

PACS number(s): 82.70.Gg, 61.25.Hq, 78.35.+c

## I. INTRODUCTION

Polymer gel is an adventurous soft matter, with many unsolved and interesting problems. The principal reason of this situation is that the available methods to characterize structure and dynamics of polymer gels are limited. Since a polymer gel is a huge macromolecule with an infinite network, its characterization should be performed by *in situ* measurements. Dynamic light scattering (DLS) is one of a few powerful tools to characterize its minute network structure non-destructively. However, difficulty in using DLS for polymer gels due to the presence of inhomogeneities was pointed out recently [1], and has not been clarified completely.

DLS study of polymer gels was introduced by Tanaka *et al.* [2]. The relaxation time obtained by DLS is usually related to the cooperative diffusion constant by Einstein-Stokes relationship [3]. Although this relationship is useful, the fact is that a static component of scattering intensity due to the static inhomogeneities in gels is inevitably included in a DLS signal. Such a static component sometimes depends strongly on the measuring position in polymer gels. Thus, for polymer gels, the time-averaged properties measured at a single position do not correspond to the ensemble-averaged properties obtained from time-averaged properties measured at many positions. This is the so-called *nonergodic problem* and it prevents us from determining correct properties of polymer gels.

To overcome this problem, several experimental and theoretical approaches have been attempted. One of the main

theoretical approaches, dynamic light-scattering theory for nonergodic media, was proposed by Pusey and van Meegen [4]. This theory is very useful and has been applied to actual DLS studies of polymer gels [5,6], although it takes no account of the position dependence of dynamic fluctuation correctly. Recently, one of the present authors has proposed another DLS theory for inhomogeneous media to derive a formula that can be applied to more general cases [7]. By using this formula, we can study various kinds of inhomogeneous gels.

To use this formula effectively, we have developed an apparatus, a scanning microscopic light-scattering (SMLS) system. By using this system, many DLS measurements can be successively performed at many positions in the sample, and the ensemble-averaged correlation function of scattering light can be calculated. With this approach, static and dynamic fluctuations in polymer gels could be observed separately in the present study and the nature of inhomogeneities of vinylpolymer gels could be elucidated.

The importance of taking into account the inhomogeneities in DLS study of polymer gels was pointed out several years ago [8]. A good deal of studies on the inhomogeneities has been carried out. For example, in the elongation experiments of gels, an abnormal butterfly pattern of scattering intensity is observed during elongation [9,10]. This result was explained not due to the usual thermal fluctuations but due to the presence of static inhomogeneities in the gels [11]. Such inhomogeneities were suggested to originate from concentration fluctuation that are frozen in the gel network structure [1]. Although a lot of information about the inhomogeneities has been reported, such information is not sufficient to know the structure, origin, and properties of the inhomogeneous gels.

---

\*Electronic address: hfurukaw@cc.tuat.ac.jp

geneities in polymer gels. In such a situation, we focus in the present paper on the nature of the inhomogeneities in vinylpolymer gels, especially on the origin of the inhomogeneities. In this respect, the gelation process of vinylpolymer gels is of crucial importance.

The gelation mechanism of vinylpolymer gels is one of the historical topics in polymer science. The gelation was explained by Flory-Stockmayer theory in the early stages of the research [12]. This theory succeeded in predicting gelation points in polycondensation reactions. However, it is not good at quantitatively estimating the properties of the gelation in vinyl-type polymerization. Later, percolation theory was introduced to estimate the gelation properties [13]. These types of theories are valid for the physical and reversible gelation processes, but can be hardly used for the non-reversible gelation with chemical cross-linking, i.e., with the formation of covalent bonds.

From another point of view, the chemical gelation with the appearance of inhomogeneous microgels has also been discussed in the synthesis of vinylpolymer gels and networks [14,15]. Concretely, the vinylpolymer gels are usually prepared by the copolymerization of a vinyl monomer and a divinyl cross-linker. Since the reactivities of monomer and cross-linker are sometimes different, the gelation process should be divided into several stages of chemical reactions. Furthermore, the reactions should be analyzed by considering the difference between inter macromolecular and intramacromolecular reactions. Although these approaches are complicated, it is necessary to correctly investigate the actual gelation processes to know the origin of the inhomogeneities.

In this context, the present authors tried to study the viscosity growth during gelation [16]. The gelation process of polyacrylamide (PAAm) gels was explained by formation of macrogel from many microgels. Moreover, one of the present authors studied the preparation-concentration dependence of swelling behavior of PAAm gels [17]. It was found that different network structures are formed depending on the monomer concentration in the preparation. The differences in the network structure were explained by the differences in gelation process. To justify such an explanation, we should collect information on various kinds of network structures by using various characterization techniques [18]. This approach could reveal the nature of the inhomogeneities.

In the present study, the network structure and inhomogeneities of PAAm gels are characterized by using a SMLS system and the general formula [7] for an ensemble-averaged correlation function. Comparing the structure and inhomogeneities between as-prepared and fully swollen states of the several gels prepared at different monomer concentrations, we try to clarify the nature of inhomogeneities in vinylpolymer gels and, especially their origin.

The format of this paper is as follows. In Sec. II, the theoretical background of DLS is explained simply and the general formula for an ensemble-averaged correlation function is derived. The sample preparation of various PAAm gels with different kinds of inhomogeneities is given in Sec. III A. The SMLS apparatus and the experimental analysis method of SMLS data are mentioned in Secs. III B and III C, respectively. The experimental results are reported in Sec. IV.

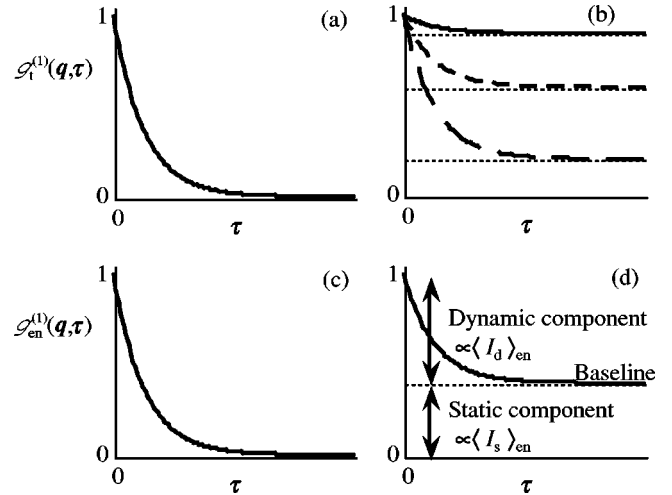


FIG. 1. Examples of first-order correlation functions. Time-averaged correlation function  $g_t^{(1)}(\mathbf{q}, \tau)$  in the absence of static fluctuation (a), and that in the presence of static fluctuation (b). Ensemble-averaged correlation function  $g_{en}^{(1)}(\mathbf{q}, \tau)$  in the absence of static fluctuation (c), and that in the presence of static fluctuation (d).

In Sec. V, the change in the structure and inhomogeneities between as-prepared and fully swollen states of the several gels are discussed and a model for the inhomogeneous gels is proposed. Conclusion is given in Sec. VI.

## II. THEORETICAL BACKGROUND OF THE DYNAMIC LIGHT SCATTERING FROM INHOMOGENEOUS MEDIA

In DLS studies, a dynamic structure factor  $f(\mathbf{q}, \tau)$  is determined from the observable properties.  $f(\mathbf{q}, \tau)$  has the meaning of an autocorrelation function of the density fluctuation in samples,  $\tau$  is the correlation time, and  $\mathbf{q}$  is the scattering vector. It can be shown that  $f(\mathbf{q}, \tau)$  is directly proportional to the first-order autocorrelation function of the scattered electric field  $E(\mathbf{q}, \tau)$  as [19]

$$f(\mathbf{q}, \tau) \sim \langle E^*(\mathbf{q}, t)E(\mathbf{q}, t + \tau) \rangle_{en} \propto g_{en}^{(1)}(\mathbf{q}, \tau), \quad (1)$$

where  $\langle \dots \rangle_{en}$  means ensemble-averaging and  $g_{en}^{(1)}(\mathbf{q}, \tau)$  is an ensemble averaged first-order autocorrelation function of  $E(\mathbf{q}, t)$

In the case of gels, we should consider a static fluctuation built-in by the concentration fluctuation during preparation reactions. Such a static fluctuation is inevitably observed by light scattering experiments of usual gels, as a “speckle pattern,” i.e., a large static component of scattering intensity that strongly depends on the measuring position in a sample. The position-dependent static fluctuation results in the fact that the time-averaged autocorrelation function obtained at one position of scattering volume,  $g_t^{(1)}(\mathbf{q}, \tau)$ , has an anomalous nonrelaxation component, called a *baseline*, which depends on the position of scattering volume in the sample, as shown in Fig. 1(b). The ensemble-averaged autocorrelation function  $g_{en}^{(1)}(\mathbf{q}, \tau)$  obtained by space averaging of a large number of  $g_t^{(1)}(\mathbf{q}, \tau)$  obtained at different positions of scat-

tering volume also has the non-relaxation component that is a unique quantity characterizing the sample as a whole, as shown in Fig. 1(d). In the present work, the properties of gels are characterized by the analysis of the ensemble-averaged correlation function  $g_{\text{en}}^{(1)}(\mathbf{q}, \tau)$ . In the following, we explain the derivation of  $g_{\text{en}}^{(1)}(\mathbf{q}, \tau)$ .

The time-averaged first-order autocorrelation function of  $E(\mathbf{q}, t)$  is defined by [20]

$$g_t^{(1)}(\mathbf{q}, \tau) \equiv \frac{\langle E^*(\mathbf{q}, t)E(\mathbf{q}, t + \tau) \rangle_t}{(\langle I(\mathbf{q}, t) \rangle_t \langle I(\mathbf{q}, t + \tau) \rangle_t)^{1/2}}, \quad (2)$$

where  $t$  denotes real time,  $I(\mathbf{q}, t)$  is the scattering intensity at  $\mathbf{q}$  and  $t$ , and  $\langle \dots \rangle_t$  means the time-averaging operation. Here “time averaging” means that the DLS measurement is carried out at one position of scattering volume in the sample and the time average of  $E^*(\mathbf{q}, t)E(\mathbf{q}, t + \tau)$  is measured on the laboratory time scale. In the actual measurements with a common self-beating (or homodyne) method, we directly measure the time-averaged autocorrelation function of  $I(\mathbf{q}, t)$ , i.e., the time-averaged second-order autocorrelation function of  $E(\mathbf{q}, t)$ , which is defined by [20]

$$g_t^{(2)}(\mathbf{q}, \tau) \equiv \frac{\langle I(\mathbf{q}, t)I(\mathbf{q}, t + \tau) \rangle_t}{\langle I(\mathbf{q}, t) \rangle_t \langle I(\mathbf{q}, t + \tau) \rangle_t}. \quad (3)$$

Since we would like to determine the dynamic structure factor from  $g_t^{(2)}(\mathbf{q}, \tau)$ , we need to relate  $g_t^{(2)}(\mathbf{q}, \tau)$  to  $g_t^{(1)}(\mathbf{q}, \tau)$ . There is a known approximate relationship between them, called Gaussian approximation, which can be used if  $E(\mathbf{q}, t)$  is the zero-mean Gaussian variables. This relationship is written as [19]

$$g_{\text{en}}^{(2)}(\mathbf{q}, \tau) = 1 + \gamma^2 [g_{\text{en}}^{(1)}(\mathbf{q}, \tau)]^2, \quad (4)$$

where  $\gamma$  ( $0 \leq \gamma \leq 1$ ) is called the coherence factor which takes into account the incoherence effect arising from the finite area of the detector. In an ideal condition  $\gamma = 1$ . This ideal condition is commonly used in DLS analysis, and is known as *Siebert relationship*. In the case of gels, however, this equation cannot be used because actual gels usually have static inhomogeneities so that the time average of  $E(\mathbf{q}, t)$  is

not zero, i.e.,  $\langle E(\mathbf{q}, t) \rangle_t \neq 0$ . In this case, we use the extended version of the Siegert relationship for inhomogeneous media, written as [4]

$$g_t^{(2)}(\mathbf{q}, \tau) = 1 + \gamma^2 [g_t^{(1)}(\mathbf{q}, \tau)]^2 - \gamma^2 [g_t^{(1)}(\mathbf{q}, \infty)]^2 \quad (5)$$

or

$$g_t^{(1)}(\mathbf{q}, \tau) = \gamma^{-1} \sqrt{1 + g_t^{(2)}(\mathbf{q}, \tau) - g_t^{(2)}(\mathbf{q}, 0)}. \quad (6)$$

In the case of homogeneous media,  $g_t^{(1)}(\mathbf{q}, \infty) = 0$  [ $g_t^{(2)}(\mathbf{q}, 0) = 2$ ] and Eq. (5) reduces to Eq. (4).

As mentioned above, in order to obtain the dynamic structure factor corresponding to the sample as a whole, the ensemble-average correlation function  $g_{\text{en}}^{(1)}(\mathbf{q}, \tau)$  should be determined [7], while taking into account the position dependence of  $g_t^{(1)}(\mathbf{q}, \tau)$  due to the inhomogeneities of gels. In actual measurements,  $g_{\text{en}}^{(1)}(\mathbf{q}, \tau)$  is calculated as the space average of the time-averaged correlation function as

$$\begin{aligned} g_{\text{en}}^{(1)}(\mathbf{q}, \tau) &\equiv \frac{\langle E^*(\mathbf{q}, t)E(\mathbf{q}, t + \tau) \rangle_{\text{en}}}{(\langle I(\mathbf{q}, t) \rangle_{\text{en}} \langle I(\mathbf{q}, t + \tau) \rangle_{\text{en}})^{1/2}} \\ &= \frac{\langle \langle E^*(\mathbf{q}, t)E(\mathbf{q}, t + \tau) \rangle_t \rangle_{\text{sp}}}{\langle I(\mathbf{q}, t) \rangle_{\text{en}}}, \end{aligned} \quad (7)$$

where  $\langle \dots \rangle_{\text{sp}}$  means space-averaging operation. By using Eqs. (2) and (6), we obtain

$$\begin{aligned} g_{\text{en}}^{(1)}(\mathbf{q}, \tau) &= \frac{\langle \langle I(\mathbf{q}, t) \rangle_t g_t^{(1)}(\mathbf{q}, \tau) \rangle_{\text{sp}}}{\langle I(\mathbf{q}, t) \rangle_{\text{en}}} \\ &= \frac{\langle \langle I(\mathbf{q}, t) \rangle_t \gamma^{-1} \sqrt{1 + g_t^{(2)}(\mathbf{q}, \tau) - g_t^{(2)}(\mathbf{q}, 0)} \rangle_{\text{sp}}}{\langle I(\mathbf{q}, t) \rangle_{\text{en}}}. \end{aligned} \quad (8)$$

It should be noted that  $g_{\text{en}}^{(1)}(\mathbf{q}, \tau) \neq \langle g_t^{(1)}(\mathbf{q}, \tau) \rangle_{\text{sp}}$ . Thus in order to calculate  $g_{\text{en}}^{(1)}(\mathbf{q}, \tau)$ , we should use Eq. (8) [7].

If one focuses only on the dynamic component of the dynamic structure factor, i.e., on the dynamics of the inhomogeneous media, the normalized dynamic component of  $g_{\text{en}}^{(1)}(\mathbf{q}, \tau)$  can be calculated by

$$\Delta g_{\text{en}}^{(1)}(\mathbf{q}, \tau) = \frac{g_{\text{en}}^{(1)}(\mathbf{q}, \tau) - g_{\text{en}}^{(1)}(\mathbf{q}, \infty)}{g_{\text{en}}^{(1)}(\mathbf{q}, 0) - g_{\text{en}}^{(1)}(\mathbf{q}, \infty)} = \frac{\langle \langle I(\mathbf{q}, t) \rangle_t \sqrt{1 + g_t^{(2)}(\mathbf{q}, \tau) - g_t^{(2)}(\mathbf{q}, 0)} \rangle_{\text{sp}} - \langle \langle I(\mathbf{q}, t) \rangle_t \sqrt{2 - g_t^{(2)}(\mathbf{q}, 0)} \rangle_{\text{sp}}}{\langle I(\mathbf{q}, t) \rangle_{\text{en}} - \langle \langle I(\mathbf{q}, t) \rangle_t \sqrt{2 - g_t^{(2)}(\mathbf{q}, 0)} \rangle_{\text{sp}}}. \quad (9)$$

Note that this equation is free from  $\gamma$ . It means that the incoherent effect need not to be taken care of in the analysis of dynamics by using Eq. (9).

Further, by using the baseline of  $g_{\text{en}}^{(1)}(\mathbf{q}, \tau)$ , we can obtain separately the static and the dynamic components,  $\langle I_s(\mathbf{q}) \rangle_{\text{en}}$  and  $\langle I_d(\mathbf{q}, t) \rangle_{\text{en}}$ , of the ensemble-averaged scattering intensity  $\langle I(\mathbf{q}, t) \rangle_{\text{en}}$ . From Fig. 1(d), we find that the heterodyne function  $g_{\text{en}}^{(1)}(\mathbf{q}, \tau)$  has a “baseline” due to the presence of

the static fluctuation. Thus we obtain the following equations [7,21]:

$$\langle I_s(\mathbf{q}) \rangle_{\text{en}} = \langle I(\mathbf{q}, t) \rangle_{\text{en}} g_{\text{en}}^{(1)}(\mathbf{q}, \infty), \quad (10)$$

$$\langle I_d(\mathbf{q}, t) \rangle_{\text{en}} = \langle I(\mathbf{q}, t) \rangle_{\text{en}} [1 - g_{\text{en}}^{(1)}(\mathbf{q}, \infty)]. \quad (11)$$

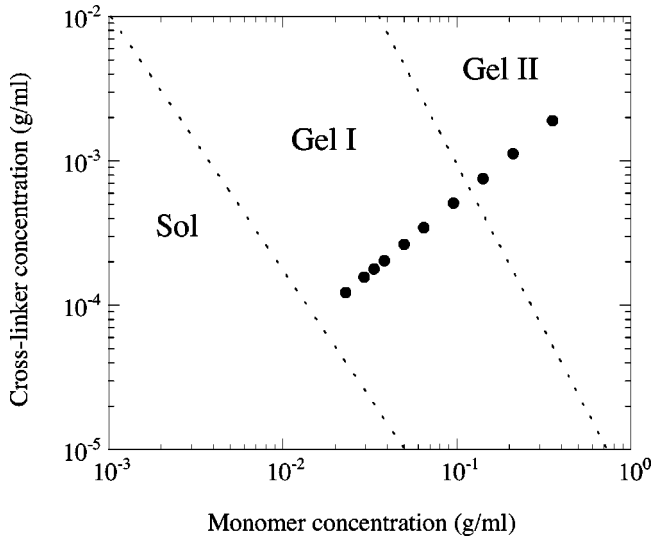


FIG. 2. The monomer composition of the gel samples prepared in the present study: Filled circles indicate the concentrations of AAm monomer and BIS cross-linker of pregel solutions. The concentration ratio of AAm to BIS is constant. The meaning of three regions is described in the text.

By using the above formulas for  $g_{\text{en}}^{(1)}(\mathbf{q}, \tau)$ ,  $\Delta g_{\text{en}}^{(1)}(\mathbf{q}, \tau)$ ,  $\langle I_s(\mathbf{q}) \rangle_{\text{en}}$ , and  $\langle I_d(\mathbf{q}, t) \rangle_{\text{en}}$ , we are able to characterize the whole properties of the inhomogeneous medium, even when it has a nonergodic nature. Especially, as described below, we can calculate an ensemble-averaged distribution function  $P_{\text{en}}(\mathbf{q}, \tau_R)$  of relaxation time  $\tau_R$  directly from  $\Delta g_{\text{en}}^{(1)}(\mathbf{q}, \tau)$  by using a kind of inverse Laplace transform method. Such a  $P_{\text{en}}(\mathbf{q}, \tau_R)$  gives full information on the dynamic fluctuation of the media. In case of polymer gels, for instance, distributions of mesh size, cluster radius, and so on are obtained. Further, from  $\langle I_s(\mathbf{q}) \rangle_{\text{en}}$  and  $\langle I_d(\mathbf{q}, t) \rangle_{\text{en}}$ , we can obtain valuable information on static and dynamic inhomogeneities in polymer gels. These are intrinsic merits of using the above equations.

### III. EXPERIMENT

#### A. Preparation of polyacrylamide gels

PAAm gels were prepared by radical copolymerization of acrylamide (AAm) monomer and *N,N'*-methylenebisacrylamide (BIS) cross-linker (Wako Chemicals Co.) in aqueous solution. The pregel solutions were prepared by varying the total monomer volume fraction in solution,  $\phi_0$ , systematically while keeping the ratio of the cross-linker to the monomer constant (BIS/AAm=0.246 mol%). At this ratio, the average number of monomer units between cross-linking points,  $N$ , becomes 200 if the reaction occurs completely.

The concentrations of the monomer and cross-linker in solutions are shown in Fig. 2. In this figure, the broken lines denote two kinds of boundaries. One indicates the sol-gel boundary. The other corresponds to the crossover between two different types of gels [17]. The differences will be explained below. The sample gels were prepared by varying the

monomer concentrations widely over these gel I and gel II regions.

In order to study the swelling-induced modulation of the gel properties, both as-prepared and equilibrium-swollen gels were prepared as follows. In order to avoid hydrolysis at room temperature, all the preparation procedures were carried out at 6.0°C. The pregel solutions were filtered with a micron filter of 0.22  $\mu\text{m}$  pore size to remove dust particles and bubbled with nitrogen to purge oxygen. To initiate redox polymerization, ammonium persulfate as an initiator and *N,N,N',N'*-tetramethylethylenediamine (Wako Chemicals Co.) as an accelerator were added to the pregel solutions at net concentrations of 0.4 mg/ml and 4  $\mu\text{l/ml}$ , respectively. Immediately after the addition, the solutions were transferred into glass tubes of 4.5 mm inner diameter for as-prepared sample gels and into glass molds of 1–3 mm inner diameter for swollen sample gels. After 24 h, the latter gels were pushed out from the molds and soaked in a large amount of water for 2 weeks at room temperature to reach the swelling equilibrium. The swollen gels were then transferred into sample glass tubes. Initially, ten types of samples were prepared. However, lower concentration gels became fragile and the lowest concentration swollen gel could not be treated easily. This gel was then excluded from the measurement of swelling ratio and SMLS.

The equilibrium swelling ratio of the swollen sample gels was determined from the diameters of the gels,  $L$ , measured with a cathetometer (accuracy 0.01 mm). Before measurements, the sample gels were kept at 30.0°C for 24 h to reach the swelling equilibrium. The apparent swelling ratio  $\alpha$  was calculated by  $\alpha = (L/L_0)^3$ , where  $L_0$  is the inner diameter of the gel mold. The actual swelling ratio  $Q$  was calculated by  $Q = 1/\phi = \alpha/\phi_0$ , where  $\phi$  is the volume fraction of total monomer units in swollen gels in equilibrium, and  $\phi_0$  is that in as-prepared gels.

The swelling behavior of the sample gels is shown in Fig. 3. The value of  $\alpha$  changes differently as a function of  $\phi_0$  in different regions. In low  $\phi_0$  region  $\alpha$  decreases sharply as  $\phi_0$  increases, while in high  $\phi_0$  region  $\alpha$  increases gradually as  $\phi_0$  increases. There is a crossover concentration between the two regions as shown in Fig. 2. The value of  $Q$  also has two kinds of  $\phi_0$  dependences and the change occurs at the crossover concentration. It has been found in our previous study [17] that this behavior is observed universally and independently of the molar ratio of the cross-linker to the monomer. The swelling behavior is described by the following experimental formula:

$$Q = A(\phi_0 - \phi_g)^{-a} e^{-\phi_0/\phi_c} + \frac{B}{1 + \left(\frac{\phi_0}{\phi_c}\right)^b}, \quad (12)$$

where  $\phi_c$  is the crossover volume fraction ( $\phi_c = 0.059$  in the present case),  $A$  and  $B$  are constants,  $\phi_g$  is the gelation volume fraction, and  $a$  and  $b$  are adjustable indices. It suggests that in each region different gels with different nature of network structure are formed. In low  $\phi_0$  region, gels may have many defects due to the fractal-like structure that forms

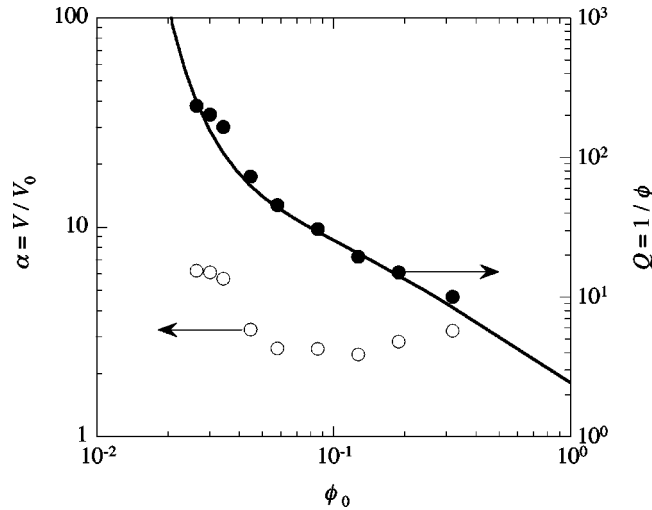


FIG. 3. The equilibrium swelling behavior of the sample gels. Open circles indicate the apparent swelling ratio  $\alpha = V/V_0$  as a function of total monomer volume fraction in preparation,  $\phi_0$ , where  $V_0$  is the volume of gel in preparation and  $V$  is that in the state of equilibrium swelling. Closed circles indicate the actual swelling ratio  $Q = 1/\phi$ , where  $\phi$  is the equilibrium volume fraction of polymer chains. The solid curves are fitted ones to the experimental formula (12) described in the text.

near the gelation point. On the other hand, in high  $\phi_0$  region, gels may have many topological entanglements among subchains of network. Then, the effective concentration of cross-linking points becomes large. In the following, we study the properties of the different types of inhomogeneities due to the different structure of networks.

### B. Scanning microscopic light scattering

In the present study, we constructed a SMLS apparatus to measure both the time course of local scattering intensity and its autocorrelation function at a large number of positions in a sample. The schematic view of SMLS is illustrated in Fig. 4. For light source, 22-mW linearly polarized He-Ne laser was used. Incident light is focused on the sample with a  $40\times$  objective lens of super-long-working distance, so that the beam diameter at scattering volume is about  $3\ \mu\text{m}$ . Scattered light passes a pinhole of  $100\text{-}\mu\text{m}$  aperture, and focused by a convex lens onto an end of optical fiber of  $100\text{-}\mu\text{m}$  aperture and 2 m length. The two apertures satisfy the coherent condition [19]. The optics is mounted on an arm of a goniometer, whose length is 30 cm. The goniometer is controlled by a personal computer (PC) (NEC, PC9821Ap2). The available scattering angle usually ranges from near  $0^\circ$  to  $145^\circ$ . The sample holder has a cylindrical shape, 5 cm in diameter. It is made of an aluminum block and has a center hole 10 mm in diameter, with a 10-mm glass tube inserted inside as an oil bath. A light-scattering cell, glass tube of 5 mm outer diameter, is immersed in the oil bath. The sample holder is moved vertically by a stepping motor with a minimum step of  $1\text{-}\mu\text{m}$ . A thermistor is set in the oil bath. The thermal controller is made of a Wheatstone bridge circuit with the thermistor and a proportional-integral-differential action circuit [22]. The temperature stability of the light-

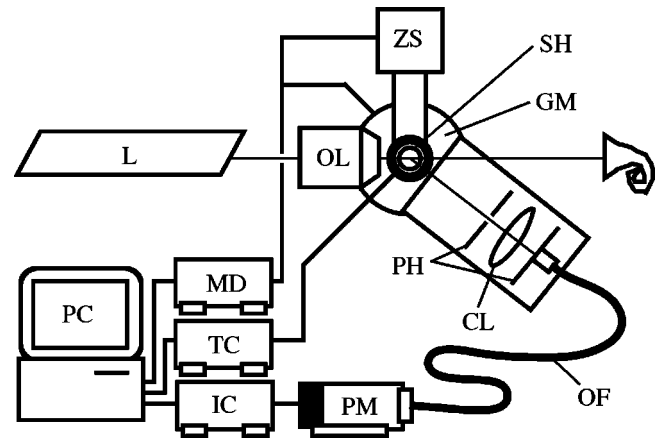


FIG. 4. Schematic of scanning microscopic light-scattering apparatus. L: laser, OL: objective lens with super-long-working distance, SH: sample holder, GM: computerized goniometer, ZS: computerized z-axis scanner, PH: pinholes, CL: convex lens, OF: optical fiber, PM: photomultiplier with preamplifier and discriminator counter, MD: stepping motor driver, TC: temperature controller and thermometer, IC: correlator (pulse interval counter), PC: personal computer.

scattering cell was better than  $0.001^\circ\text{C}$ . The scattered light is detected as a train of photon pulses with a photomultiplier (Hamamatsu Photonics, R649S) and input to the PC with a sample laboratory-made correlator, which measures intervals between the photon pulses with a 10-MHz crystal oscillator as a time scaler. The correlation function was calculated by using a software which counts the frequency distribution (frequency histogram) of the intervals between the photon pulses and provides the frequency curve of the intervals as a correlation function [23].

### C. Characterization of ensemble-averaged correlation functions

In the present work, the dynamic component of the ensemble-averaged correlation function,  $\Delta g_{\text{en}}^{(1)}(\tau)$ , was analyzed with a kind of inverse Laplace transform (ILT) method. In general,  $\Delta g_{\text{en}}^{(1)}(\tau)$  can be approximately expressed by a superposition of many exponential functions as [24,25]

$$\Delta g_{\text{en}}^{(1)}(\tau) = N \sum_{i=1}^n P_{\text{en}}(\ln \tau_{R,i}) \exp\left(-\frac{\tau}{\tau_{R,i}}\right), \quad (13)$$

where  $\{\tau_{R,i}\}$  is a geometric progression of relaxation time expressed as

$$\tau_{R,i} = \tau_{R,\min} (\tau_{R,\max} / \tau_{R,\min})^{(i-1)/n} \quad (i=1, 2, \dots, n) \quad (14)$$

and  $N$  is a normalized factor defined as

$$N = \frac{1}{n} \ln \frac{\tau_{R,\max}}{\tau_{R,\min}}. \quad (15)$$

Here, it is easy to check that  $P_{\text{en}}(\ln \tau_{R,i})$  satisfies

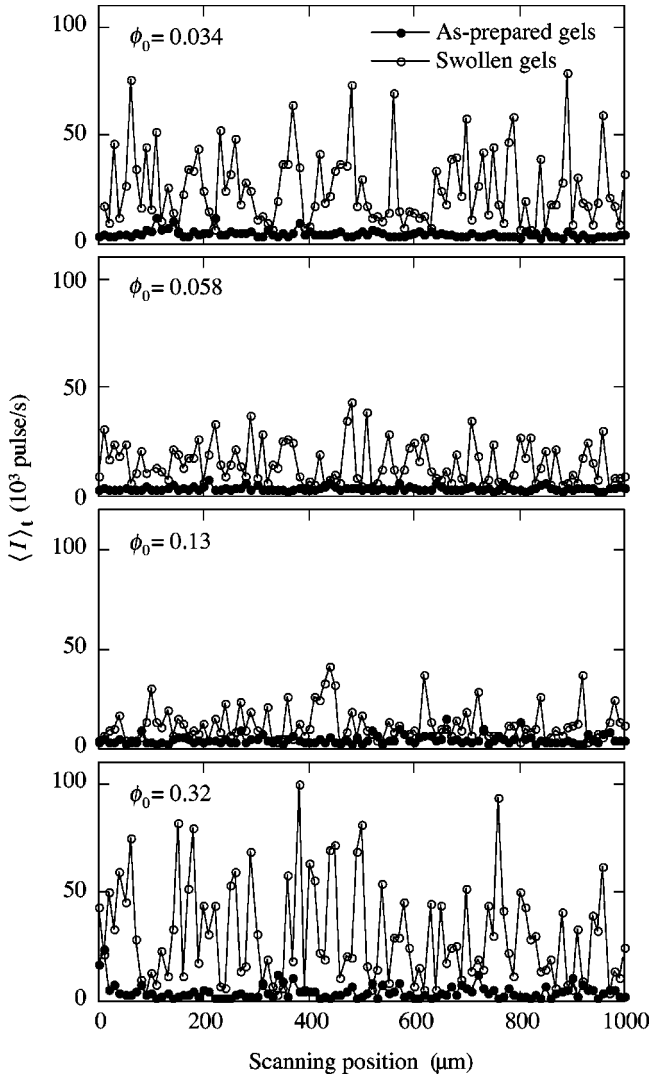


FIG. 5. The position dependence of the time-averaged scattering intensity  $\langle I(\mathbf{q}, t) \rangle_t$ . The scattering angle is  $\theta = 60^\circ$ . Here  $\phi_0$  is the volume fraction of monomer and cross-linker in preparation.

$$\int_{\ln \tau_{R,\min}}^{\ln \tau_{R,\max}} P_{\text{en}}(\ln \tau_R) d \ln \tau_R = \sum_{i=1}^n P_{\text{en}}(\ln \tau_{R,i}) \frac{\ln \tau_{R,\max} - \ln \tau_{R,\min}}{n} = 1. \quad (16)$$

where we have used Eq. (13) in setting  $\tau = 0$ .

By using Eq. (13), we can obtain the distribution function of relaxation time,  $P_{\text{en}}(\ln \tau_R)$ , directly from  $\Delta g_{\text{en}}^{(1)}(\tau)$ . Thus, in the present study, the nonlinear least squares fitting of  $\Delta g_{\text{en}}^{(1)}(\tau)$  to the right-hand side of Eq. (13) was performed where  $\{P_{\text{en}}(\ln \tau_{R,i})\}$  was treated as a set of fitting parameters. The fitting was performed with  $\tau_{R,\min} = 10^{-6}$  s,  $\tau_{R,\max} = 10^1$  s, and  $n = 70$  for all cases of ILT analysis in the present work.

#### IV. RESULTS OF SMLS MEASUREMENTS

Figure 5 shows the swelling-induced fluctuation and growth of the time-averaged intensity  $\langle I(\mathbf{q}, t) \rangle_t$  for the

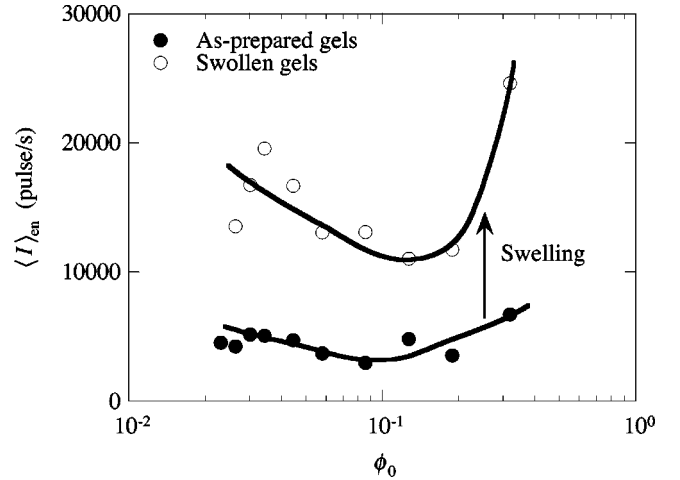


FIG. 6. The ensemble-averaged scattering intensity  $\langle I(\mathbf{q}, t) \rangle_{\text{en}}$  as a function of the volume fraction of total monomer units in preparation,  $\phi_0$ , for both as-prepared and equilibrium swollen gels. The scattering angle is  $60^\circ$ . The solid curves are guides to the eye.

PAAm gels. These results were obtained by  $10\text{-}\mu\text{m}$  step scanning measurements of the gels in both as-prepared and equilibrium swollen states.  $\langle I(\mathbf{q}, t) \rangle_t$  was measured at each position of the gel and plotted in Fig. 5 as a function of the scanning position.  $\phi_0$  in Fig. 5 is the volume fraction of monomer and cross-linker at the time of preparation, i.e., the volume fraction of the gel in the as-prepared state. Each plot indicates the position dependence of  $\langle I(\mathbf{q}, t) \rangle_t$  in the equilibrium swollen state as well as in the as-prepared state for gels prepared at the same  $\phi_0$ . Such a position dependence is often called a speckle pattern [8].

For small  $\phi_0$  ( $\phi_0 = 0.034$ ), where  $\alpha \approx 6$ , the swelling-induced growth of  $\langle I(\mathbf{q}, t) \rangle_t$  is strong. For intermediate  $\phi_0$  ( $\phi_0 = 0.058$  and  $\phi_0 = 0.13$ ), where  $\alpha = 2-3$ , the growth of  $\langle I(\mathbf{q}, t) \rangle_t$  is weak. Further, for large  $\phi_0$  ( $\phi_0 = 0.32$ ), where  $\alpha \geq 3$ , the growth of  $\langle I(\mathbf{q}, t) \rangle_t$  is again strong. The comparison of the landscapes of the speckle patterns shows that the notches are narrow and deep for large  $\phi_0$ , and for small  $\phi_0$  the valleys have sometimes flat regions.

Figure 6 shows the  $\phi_0$  dependence of the ensemble-averaged scattering intensity  $\langle I(\mathbf{q}, t) \rangle_{\text{en}}$  for both as-prepared and equilibrium swollen gels. Here  $\langle I(\mathbf{q}, t) \rangle_{\text{en}}$  was calculated as  $\langle I(\mathbf{q}, t) \rangle_{\text{en}} = \langle \langle I(\mathbf{q}, t) \rangle_t \rangle_{sp}$ . For as-prepared gels,  $\langle I(\mathbf{q}, t) \rangle_{\text{en}}$  has a minimum in the intermediate  $\phi_0$  region. As gels become swollen,  $\langle I(\mathbf{q}, t) \rangle_{\text{en}}$  increases and the  $\phi_0$  dependence of  $\langle I(\mathbf{q}, t) \rangle_{\text{en}}$  is more pronounced. For the swollen gels,  $\langle I(\mathbf{q}, t) \rangle_{\text{en}}$  has again a minimum in the intermediate  $\phi_0$  region. However, the minimum is shifted to a higher value. For the largest  $\phi_0$  ( $\phi_0 = 0.32$ ),  $\langle I(\mathbf{q}, t) \rangle_{\text{en}}$  in the swollen state has a maximum value.

Figure 7 shows ensemble-averaged autocorrelation functions  $g_{\text{en}}^{(1)}(\mathbf{q}, \tau)$  of the PAAm gels.  $g_{\text{en}}^{(1)}(\mathbf{q}, \tau)$  was calculated using Eq. (8) from more than a hundred  $g_t^{(2)}(\mathbf{q}, \tau)$ 's measured at different positions. Hence  $g_{\text{en}}^{(1)}(\mathbf{q}, \tau)$  gives unique information specific to each gel independent of measured positions. Each  $g_{\text{en}}^{(1)}(\mathbf{q}, \tau)$  reflects a relaxation process atop a non-decaying baseline. This relaxation corresponds to the

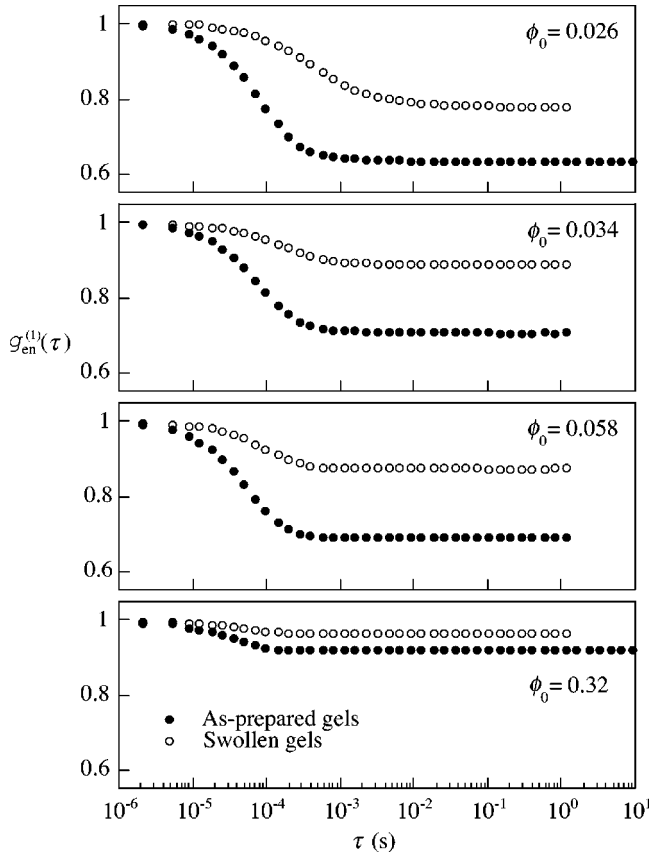


FIG. 7. The ensemble-averaged autocorrelation functions  $g_{\text{en}}^{(1)}(\mathbf{q}, \tau)$  for both as-prepared and equilibrium swollen gels. The scattering angle is  $60^\circ$ . Here  $\phi_0$  is the volume fraction of total monomer units in the as-prepared gels.

so-called “gel mode.” The term seems to be somewhat broad and the process may not be expressed by a single exponential decay. The relaxation time will be analyzed in detail below. Here, we cannot think of any other relaxation process instead of the gel mode. The baseline of  $g_{\text{en}}^{(1)}(\mathbf{q}, \tau)$  depends on  $\phi_0$  and its level increases with swelling.

From  $\langle I(\mathbf{q}, t) \rangle_{\text{en}}$  and  $g_{\text{en}}^{(1)}(\mathbf{q}, \tau)$  (shown in Figs. 6 and 7), the static and dynamic components of  $\langle I(\mathbf{q}, t) \rangle_{\text{en}}$ ,  $\langle I_s(\mathbf{q}) \rangle_{\text{en}}$  and  $\langle I_d(\mathbf{q}, t) \rangle_{\text{en}}$  were calculated by using Eqs. (10) and (11), respectively. In Fig. 8,  $\langle I_s(\mathbf{q}) \rangle_{\text{en}}$  and  $\langle I_d(\mathbf{q}, t) \rangle_{\text{en}}$  are plotted as a function of the volume fraction at the time of measurement, i.e., as a function of  $\phi_0$  for the as-prepared gels and  $\phi$  for the equilibrium swollen gels. This figure shows the values for several scattering angles, i.e.,  $\theta = 40, 60$ , and  $95^\circ$ .

It was found that the dynamic component  $\langle I_d(\mathbf{q}, t) \rangle_{\text{en}}$  is well scaled by a power function of the volume fraction at the time of measurement, which is shown by a solid line in the figure. The scattering angle dependence of  $\langle I_d(\mathbf{q}, t) \rangle_{\text{en}}$  seems to be weak and there seems to be little difference between as-prepared and swollen gels. On the other hand, the profile of the static component  $\langle I_s(\mathbf{q}) \rangle_{\text{en}}$  is different between the as-prepared and the equilibrium swollen gels. For as-prepared gels,  $\langle I_s(\mathbf{q}) \rangle_{\text{en}}$  only weakly depends on  $\phi_0$ . There is a minimum in an intermediate  $\phi_0$  region, similar to the case of  $\langle I(\mathbf{q}, t) \rangle_{\text{en}}$  shown in Fig. 6. Moreover, the scattering angle

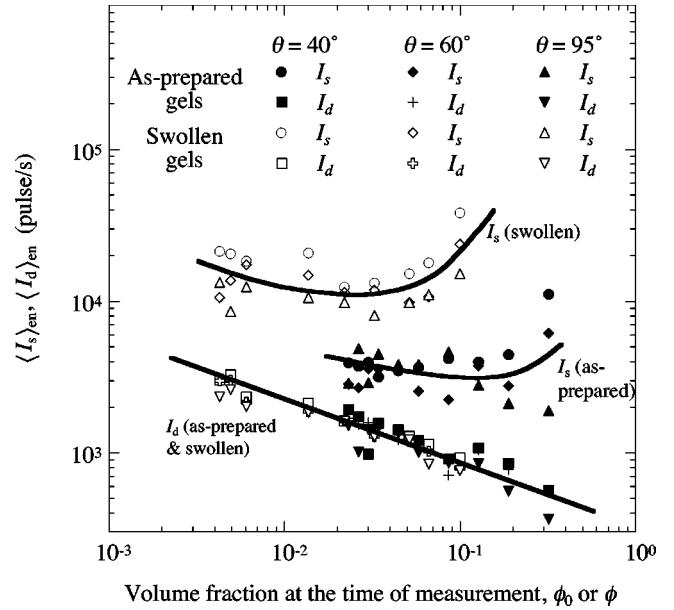


FIG. 8. The static and dynamic components of the ensemble-averaged scattering intensity,  $\langle I_s(\mathbf{q}) \rangle_{\text{en}}$  and  $\langle I_d(\mathbf{q}, t) \rangle_{\text{en}}$ , respectively, as a function of the volume fraction at the time of measurement,  $\phi_0$  (for as-prepared gels) or  $\phi$  (for equilibrium swollen gels). The closed symbols indicate the values for as-prepared gels. The open symbols indicate the values for equilibrium swollen gels. The solid line and curves are guides to the eye.

dependence seems to be somewhat strong for the largest  $\phi_0$  ( $\phi_0 = 0.32$ ), while it is rather weak for the other  $\phi_0$ . Further, for equilibrium swollen gels,  $\langle I_s(\mathbf{q}) \rangle_{\text{en}}$  strongly depends on  $\phi$  and there is a minimum of  $\langle I_s(\mathbf{q}) \rangle_{\text{en}}$  in the intermediate  $\phi$  region. The scattering angle dependence seems to be weak.  $\langle I_s(\mathbf{q}) \rangle_{\text{en}}$  has a maximum value for the largest  $\phi$ , which is also similar to the behavior of  $\langle I(\mathbf{q}, t) \rangle_{\text{en}}$  shown in Fig. 6.

In the following, the detailed analysis of dynamics in the PAAm gels is explained. The dynamic component  $\Delta g_{\text{en}}^{(1)}(\mathbf{q}, \tau)$  was calculated based on Eq. (9). The scattering angle dependence of  $\Delta g_{\text{en}}^{(1)}(\mathbf{q}, \tau)$  at  $\phi_0 = 0.086$  is shown in Fig. 9. As the scattering angle increases, the characteristic time of the relaxation process is shifted to the left, i.e., the shorter times. Moreover, the relaxation time is shifted to the right by swelling.

By using the ILT analysis as explained in Sec. III C, the distribution function  $P_{\text{en}}(\mathbf{q}, \tau_R)$ , of the relaxation time  $\tau_R$  is obtained from  $\Delta g_{\text{en}}^{(1)}(\mathbf{q}, \tau)$ . For example, the scattering angle dependence of  $P_{\text{en}}(\mathbf{q}, \tau_R)$  is shown in Fig. 10.  $P_{\text{en}}(\mathbf{q}, \tau_R)$  was calculated from  $\Delta g_{\text{en}}^{(1)}(\mathbf{q}, \tau)$  as shown in Fig. 9. We can see both  $\theta$  dependence and swelling effect on  $P_{\text{en}}(\mathbf{q}, \tau_R)$  clearly. For the quantitative analysis of dynamics,  $P_{\text{en}}(\mathbf{q}, \tau_R)$  was fitted to a logarithmic Gaussian distribution as

$$P_{\text{en}}(\mathbf{q}, \tau_R) = A \exp \left[ -\frac{(\log_{10} \tau_R - \mu)^2}{2\sigma^2} \right], \quad (17)$$

where  $A$  is the amplitude,  $\mu$  is the average of the logarithmic relaxation time, and  $\sigma^2$  is the dispersion. From  $\sigma$ , the distribution width of the relaxation time can be estimated. In Fig.

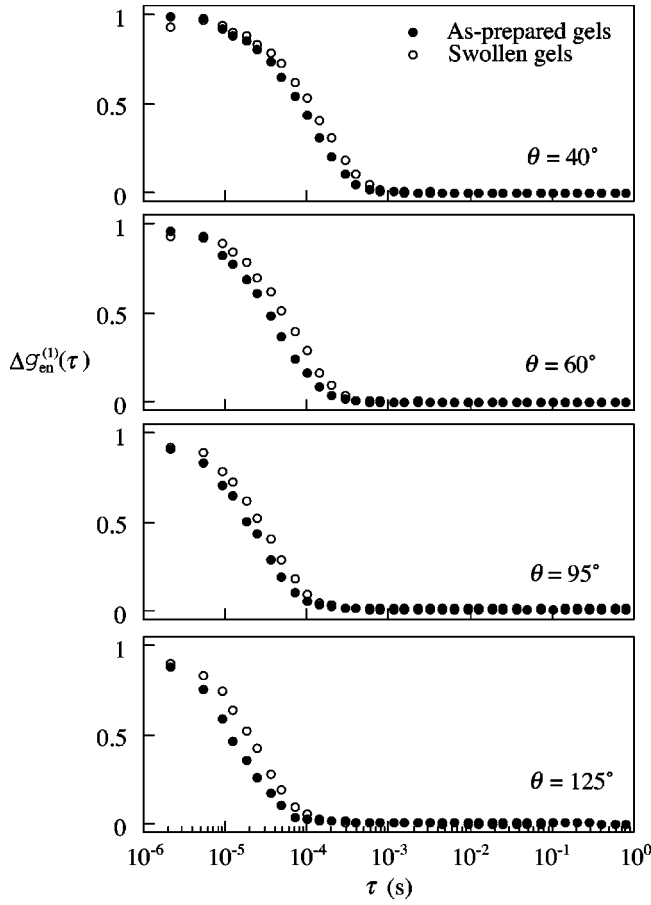


FIG. 9. An example of the scattering angle dependence of  $\Delta g_{\text{en}}^{(1)}(\mathbf{q}, \tau)$ , the dynamic component of the ensemble-averaged autocorrelation function. In each plot,  $\theta$  is the scattering angle.  $\Delta g_{\text{en}}^{(1)}(\mathbf{q}, \tau)$  was obtained for as-prepared and equilibrium swollen gels prepared at  $\phi_0 = 0.086$ .

10, the solid curves indicate the fitting results with Eq. (17). The fitting goes well as shown in Fig. 10.

From the fitting analysis with Eq. (17), the average relaxation time was given by  $\langle \tau_R \rangle = 10^\mu$  and its standard deviation  $\delta(\langle \tau_R \rangle)$  was given by  $\langle \tau_R \rangle \pm \delta(\langle \tau_R \rangle) = 10^{\mu \pm \sqrt{2}\sigma}$ . For example,  $\langle \tau_R \rangle$  of the gel prepared at  $\phi_0 = 0.086$  is shown in Fig. 11. Here, the scattering angle dependence of  $\langle \tau_R \rangle$  is shown with the absolute value of scattering vector  $q$ .  $q$  is defined by  $q = (4\pi n/\lambda)\sin(\theta/2)$ , where  $n$  is the refractive index of the sample solution,  $\lambda$  is the wavelength in a vacuum of the incident beam, and  $\theta$  is the scattering angle. If the dynamics is induced by the diffusion process,  $\langle \tau_R \rangle = q^{-2} D_{\text{coop}}^{-1}$ , where  $D_{\text{coop}}$  is the cooperative diffusion coefficient. The  $q$  dependence of  $\langle \tau_R \rangle$  was fitted to a power-law function, as is shown in Fig. 11. The slope was found to correspond approximately to  $-2$  for both the as-prepared and the equilibrium swollen gels.

Figure 12 presents the  $q^2$ -scaled plot of  $\Delta g_{\text{en}}^{(1)}(\mathbf{q}, q^2 \tau)$ . It was found that the  $q^2$ -scaled  $\Delta g_{\text{en}}^{(1)}(\mathbf{q}, q^2 \tau)$  converges well onto a master curve. It means that the relaxation of  $\Delta g_{\text{en}}^{(1)}(\mathbf{q}, \tau)$  can be well explained by the diffusion process.

Further, for each sample,  $D_{\text{coop}}$  was calculated from  $\langle \tau_R \rangle$  determined at  $\theta = 60^\circ$ . The  $\phi$  or  $\phi_0$  dependence of  $D_{\text{coop}}$  is

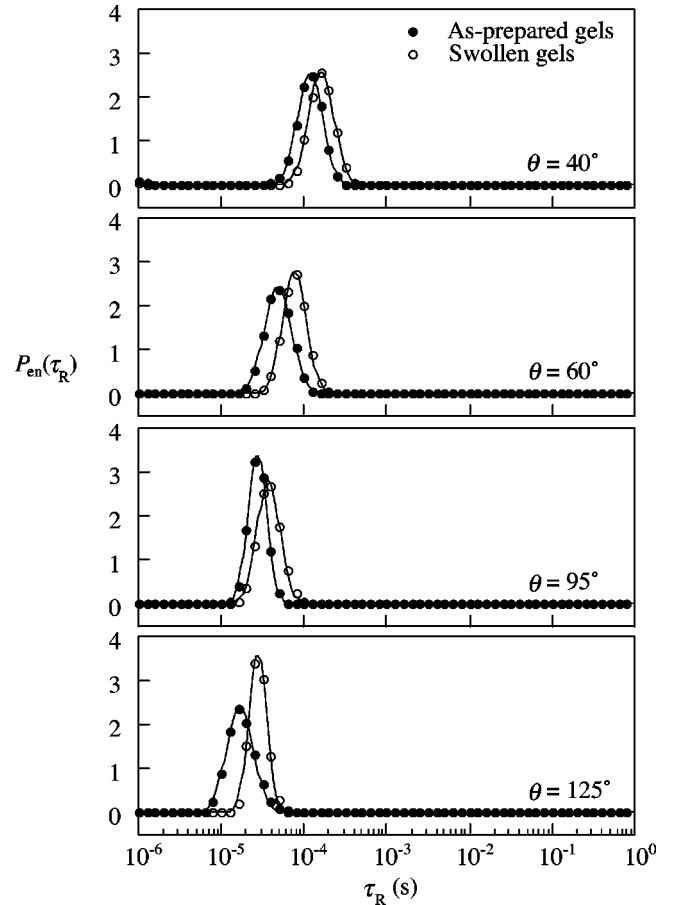


FIG. 10. An example of the scattering angle dependence of  $P_{\text{en}}(\mathbf{q}, \tau_R)$ , the distribution function of relaxation time. Here  $\theta$  is the scattering angle. The  $P_{\text{en}}(\mathbf{q}, \tau_R)$  was obtained for as-prepared and equilibrium swollen gels prepared at  $\phi_0 = 0.086$ .

plotted in Fig. 13. It is found that both  $D_{\text{coop}}$  of the as-prepared and the equilibrium swollen gels are fitted well to a power law function except for two data points of the lowest  $\phi$  and one data point of the highest  $\phi_0$ . From the fitting, the slope of the power-law of 0.51 is obtained. According to the blob theory [3], the  $\phi$  dependence of  $D_{\text{coop}}$  for semidilute polymer solutions is given by  $D_{\text{coop}} \sim \phi^{\nu/(3\nu-1)}$ , where  $\nu$  is the exponent of Flory radius;  $\nu = 3/4$  for a good solvent and  $\nu = 0.5$  for a  $\Theta$  solvent. Thus, for a good solvent  $D_{\text{coop}} \sim \phi^{0.75}$ , and for a  $\Theta$  solvent  $D_{\text{coop}} \sim \phi^{1.0}$ . However, the obtained value of 0.51 is rather small compared to these exponents. The reason of this discrepancy will be discussed in Sec. V C in detail. The right vertical axis of Fig. 13 indicates the blob size of gel network,  $\xi_{\text{blob}}$ , which was estimated by using Einstein-Stokes relationship,  $D_{\text{coop}} \approx k_B T / (3\pi\eta\xi_{\text{blob}})$ , where  $k_B$  is the Boltzmann constant,  $T$  is the absolute temperature, and  $\eta$  is the viscosity of the solvent. As seen from Fig. 13, the values of  $\xi_{\text{blob}}$  range from 3 to 60 nm, which corresponds to the mesh size of the network.

In order to observe the swelling-induced change in dynamics of the gels, the distribution functions of the relaxation time,  $P_{\text{en}}(\mathbf{q}, \tau_R)$ , were obtained for all the samples at the same scattering angle of  $\theta = 60^\circ$ , as shown in Fig. 14. From these results, it was found that the width of the  $\tau_R$

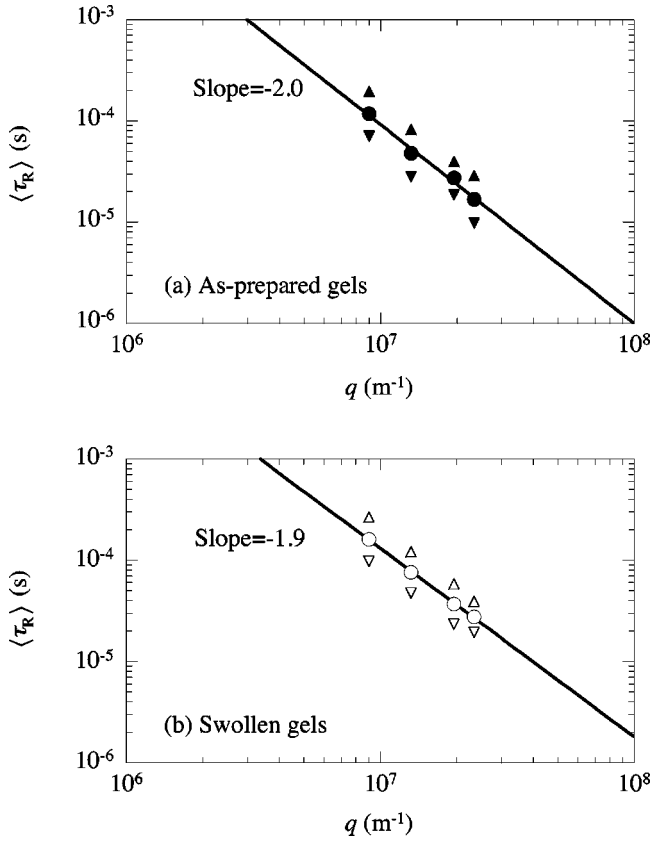


FIG. 11. The relaxation time  $\langle \tau_R \rangle$  (circles), as a function of the absolute values of scattering vector  $q$  of the gels prepared at  $\phi_0 = 0.086$ . The solid lines indicate power-law functions, to which the sets of  $\langle \tau_R \rangle$  were fitted. The triangles indicate the standard deviation of  $\langle \tau_R \rangle$ .

distribution increases with swelling. To analyze such broadening, these  $P_{en}(\mathbf{q}, \tau_R)$  were fitted with Eq. (17) and the width of the distribution of the relaxation time was estimated from  $\sigma$ . Note that for the swollen gel of  $\phi_0 = 0.026$ ,  $P_{en}(\mathbf{q}, \tau_R)$  shows bimodal distribution with two peaks. One

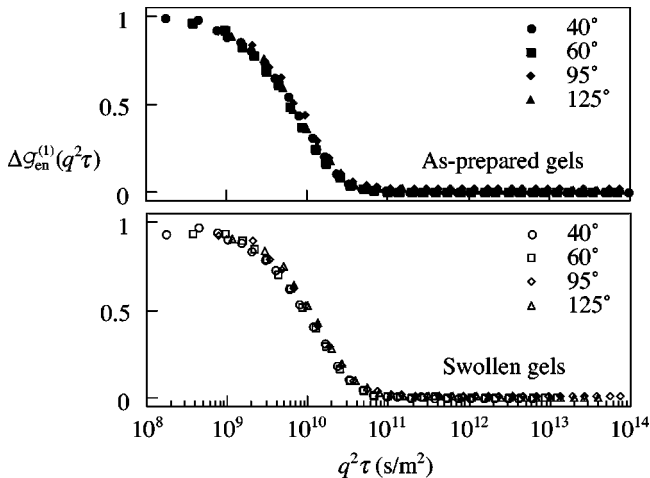


FIG. 12. The  $q^2$ -scaled correlation functions  $\Delta g_{en}^{(1)}(\mathbf{q}, q^2 \tau)$  were plotted for as-prepared and equilibrium swollen gels, which were prepared at  $\phi_0 = 0.086$ .

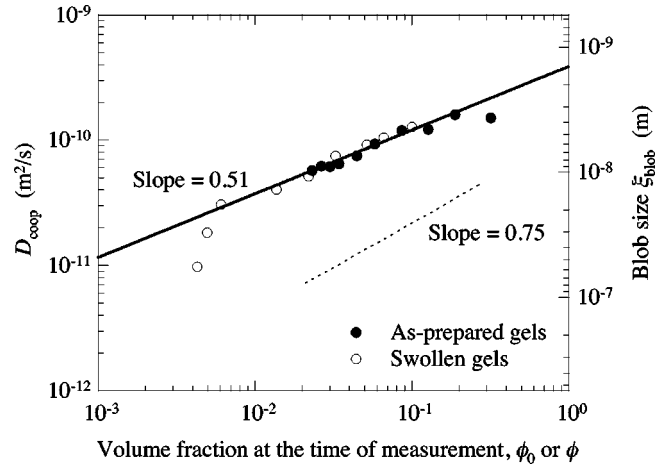


FIG. 13. The cooperative diffusion coefficient,  $D_{coop}$  as a function of the volume fraction at the time of measurement,  $\phi_0$  (for as-prepared gels) or  $\phi$  (for equilibrium swollen gels). The solid line is a power-law function fitted to the data.

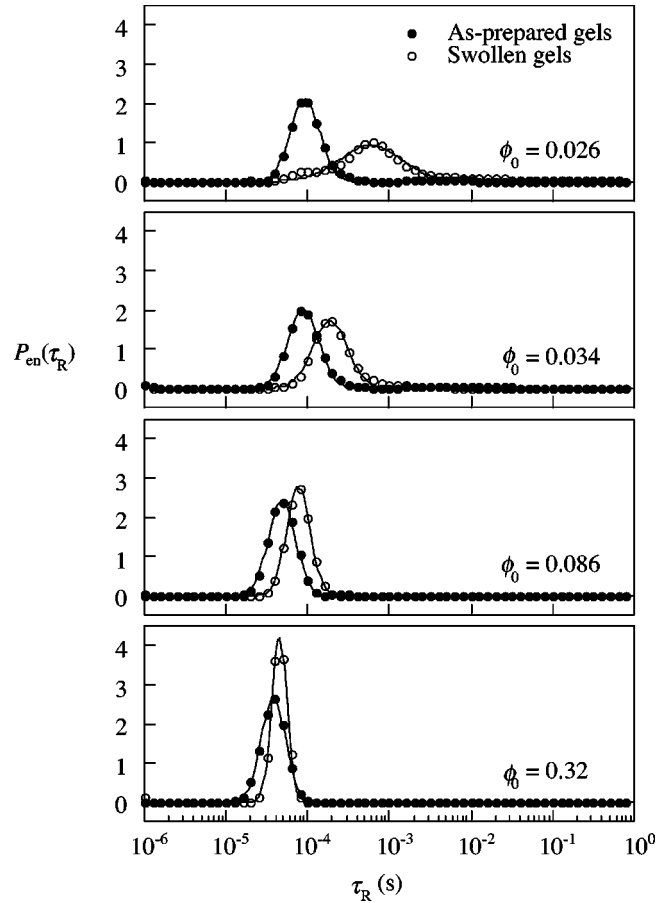


FIG. 14. Examples of the swelling-induced change of  $P_{en}(\mathbf{q}, \tau_R)$ , the distribution function of the relaxation time  $\tau_R$ . Here  $\phi_0$  is the volume fraction of total monomer units in preparation. All  $P_{en}(\mathbf{q}, \tau_R)$  were obtained at the same scattering angle of  $\theta = 60^\circ$ . Solid curves are fitted ones to Eq. (17).

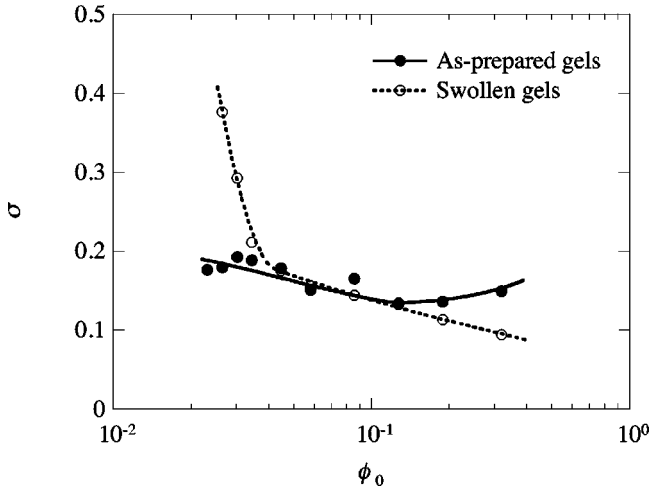


FIG. 15. The swelling-induced change in the broadness of the relaxation time. Here the distribution width of the relaxation time,  $\sigma$ , is plotted as a function of the volume fraction of total monomer units in preparation,  $\phi_0$ . The solid and broken curves are guides to the eye.

of the peaks is large and placed at slower relaxation time as compared with the peak of the as-prepared gel. The other peak is very small and placed at the same relaxation time as the peak of the as-prepared gel.

Figure 15 shows the swelling-induced change in the relaxation width  $\sigma$ . For as-prepared gels,  $\sigma$  indicates a weak dependence on  $\phi_0$  and has a minimum at an intermediate  $\phi_0$ . For equilibrium swollen gels,  $\phi_0$  dependence of  $\sigma$  becomes significant. In low  $\phi_0$  region,  $\sigma$  increases markedly by swelling. For  $\phi_0 < 0.04$ ,  $\sigma$  decreases steeply as  $\phi_0$  increases. As mentioned in Sec. III A, the lowest  $\phi_0$  gel is so fragile in the swollen state that its SMLS measurement could

not be performed. In high  $\phi_0$  region,  $\sigma$  decreases by swelling and, for  $\phi_0 > 0.04$ ,  $\sigma$  behaves as a decreasing power-law function. It means that the distribution of the relaxation modes sharpens by swelling in gels prepared at high concentrations. The data point to a large qualitative difference between the two  $\phi_0$  regions, which will be discussed in Sec. V C.

## V. DISCUSSION

### A. Difference between time-averaged correlation function and ensemble-averaged one

As mentioned in Sec. I, in order to overcome the nonergodic problem with the DLS of inhomogeneous media, several approaches have been performed. Pusey–van Megen equation [4] was proposed and has been sometimes used for solving the problem [5,6]. Pusey–van Megen equation is written as [4]

$$g_{\text{en,PM}}^{(1)}(\mathbf{q}, \tau) = \frac{(Y-1) + \sqrt{1 + g_t^{(2)}(\mathbf{q}, \tau) - g_t^{(2)}(\mathbf{q}, 0)}}{Y}, \quad (18)$$

where

$$Y \equiv \frac{\langle I(\mathbf{q}, t) \rangle_{\text{en}}}{\langle I(\mathbf{q}, t) \rangle_t}. \quad (19)$$

This equation can be derived based on the assumption that static component of fluctuation depends on position while the dynamic component does not depend on position [7]. The dynamic component of the ensemble-averaged correlation function,  $\Delta g_{\text{en,PM}}^{(1)}(\mathbf{q}, \tau)$ , is written by using this Pusey–van Megen equation as

$$\Delta g_{\text{en,PM}}^{(1)}(\mathbf{q}, \tau) = \frac{g_{\text{en,PM}}^{(1)}(\mathbf{q}, \tau) - g_{\text{en,PM}}^{(1)}(\mathbf{q}, \infty)}{g_{\text{en,PM}}^{(1)}(\mathbf{q}, 0) - g_{\text{en,PM}}^{(1)}(\mathbf{q}, \infty)} = \frac{\sqrt{1 + g_t^{(2)}(\mathbf{q}, \tau) - g_t^{(2)}(\mathbf{q}, 0)} - \sqrt{1 + g_t^{(2)}(\mathbf{q}, \infty) - g_t^{(2)}(\mathbf{q}, 0)}}{1 - \sqrt{1 + g_t^{(2)}(\mathbf{q}, \infty) - g_t^{(2)}(\mathbf{q}, 0)}}. \quad (20)$$

On the other hand, by using the extended version of Sigert equation (6), the dynamic component of time-averaged correlation function,  $\Delta g_t^{(1)}(\mathbf{q}, \tau)$ , is calculated as

$$\Delta g_t^{(1)}(\mathbf{q}, \tau) = \frac{g_t^{(1)}(\mathbf{q}, \tau) - g_t^{(1)}(\mathbf{q}, \infty)}{g_t^{(1)}(\mathbf{q}, 0) - g_t^{(1)}(\mathbf{q}, \infty)} = \frac{\sqrt{1 + g_t^{(2)}(\mathbf{q}, \tau) - g_t^{(2)}(\mathbf{q}, 0)} - \sqrt{1 + g_t^{(2)}(\mathbf{q}, \infty) - g_t^{(2)}(\mathbf{q}, 0)}}{1 - \sqrt{1 + g_t^{(2)}(\mathbf{q}, \infty) - g_t^{(2)}(\mathbf{q}, 0)}}. \quad (21)$$

Then, we can see that  $\Delta g_{\text{en,PM}}^{(1)}(\mathbf{q}, \tau) = \Delta g_t^{(1)}(\mathbf{q}, \tau)$  basically. It means that  $g_{\text{en,PM}}^{(1)}(\mathbf{q}, \tau)$  may change with measuring positions, if  $g_t^{(1)}(\mathbf{q}, \tau)$  depends on position.

Figure 16 shows several profiles of  $\Delta g_{\text{en,PM}}^{(1)}(\mathbf{q}, \tau)$  measured at different positions in a swollen gel. It is found that  $\Delta g_{\text{en,PM}}^{(1)}(\mathbf{q}, \tau)$  depends on the position, suggesting that the dynamic fluctuation in this case depends on the position. As is seen in Fig. 16,  $\Delta g_{\text{en,PM}}^{(1)}(\mathbf{q}, \tau)$  with the slowest relaxation time is a few times as slow as that with the fastest one.

Therefore, when the dynamic fluctuation is calculated from a time-averaged correlation function at a measuring position,  $g_t^{(2)}(\mathbf{q}, \tau)$ , by using Pusey–van Megen equation (20), the exact dynamic fluctuation characterizing the whole of the sample gel may not be observed.

On the other hand, the generalized equation (8) can provide rigorously an ensemble-averaged correlation function, even if the dynamic fluctuation depends on the position [7]. In Fig. 16, a dynamic component of an ensemble-averaged

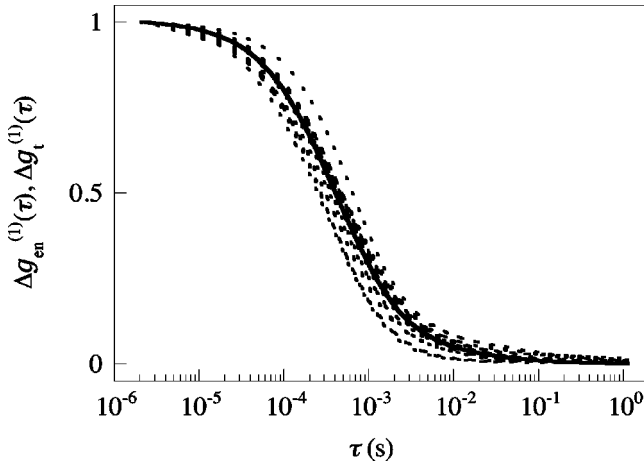


FIG. 16. The comparison of a dynamic component of an ensemble-averaged correlation function,  $\Delta g_{\text{en}}^{(1)}(\mathbf{q}, \tau)$ , (a solid curve) with those of time-averaged correlation functions at several measuring positions,  $\Delta g_t^{(1)}(\mathbf{q}, \tau)$ , (broken curves). These were obtained for an equilibrium swollen gel prepared at  $\phi_0 = 0.026$ . The scattering angle is  $60^\circ$ .

correlation function for the same gel,  $\Delta g_{\text{en}}^{(1)}(\mathbf{q}, \tau)$ , is shown from the calculation using the general equation (9). It can be seen that  $\Delta g_{\text{en}}^{(1)}(\mathbf{q}, \tau)$  obviously reflects the profiles of several  $\Delta g_t^{(1)}(\mathbf{q}, \tau)$ , and the profile of  $\Delta g_{\text{en}}^{(1)}(\mathbf{q}, \tau)$  ranges over the entire  $\Delta g_t^{(1)}(\mathbf{q}, \tau)$ . It means that  $g_{\text{en}}^{(1)}(\mathbf{q}, \tau)$  contains much more exact information on the whole properties of the gel, rather than  $g_{\text{en,PM}}^{(1)}(\mathbf{q}, \tau)$  does.

Moreover, there may be a spatial correlation between  $g_t^{(1)}(\mathbf{q}, \tau)$  and  $\langle I(\mathbf{q}, t) \rangle_t$  in inhomogeneous media. From the standpoint that such a spatial correlation relates to the properties of the inhomogeneous media, the detailed analysis of the spatial correlation can illuminate unsolved problems concerning polymer gels. We are now studying the spatial correlation in poly(*N*-isopropylacrylamide) gels. The detailed results and discussion about this will be reported elsewhere.

### B. The swelling-induced modulation of the static fluctuation

In recent years, the static fluctuation in polymer gels has become a fundamental topic of research [8]. To elucidate its origin, scattering experiments on uniaxially extended gels have been performed [1]. When such experimental results are compared to theoretical predictions, it should be kept in mind that the static fluctuations result from frozen inhomogeneities which have been introduced by the concentration fluctuation of cross-linking points in preparation and are memorized forever with covalent bonds in their network structure. Although the origin has been understood qualitatively, the nature of the static fluctuations has yet to be fully understood.

In an attempt to shed some light on the problem, we studied here the swelling-induced modulation of the static fluctuations. In a previous study by Furukawa [17], it was concluded that different types of network structure of polyacrylamide gels are prepared at low and high concentrations of total monomer units. Hence, it can be expected that

different types of gels will exhibit different behavior of static intensities when observed with SMLS.

In fact, some differences for gels with low and high concentrations of total monomer units in preparation were observed in the analysis of the scattering intensities. For low  $\phi_0$  gels, the landscape of position dependence of  $\langle I(\mathbf{q}, t) \rangle_t$ , i.e., speckle pattern (Fig. 5), and hence  $\langle I_s(\mathbf{q}) \rangle_{\text{en}}$  (Fig. 8) increase by swelling. As  $\phi_0$  decreases, the extent of the increase becomes larger (Fig. 6). Such a behavior is consistent with the predicted network structure mentioned in Sec. III A. It means that the gels prepared in low  $\phi_0$  region have many defects in their network structure and the inhomogeneities due to such defects are enlarged by swelling [9,10]. Since  $\alpha$  increases as  $\phi_0$  decreases (Fig. 3), the swelling-induced increase in inhomogeneity becomes large as  $\phi_0$  decreases.

For high  $\phi_0$  gels, strong scattering angle dependence of  $I_s$  for as-prepared states was observed (Fig. 8). This and the strong speckle pattern induced by swelling (Fig. 5) could mean that the characteristic length of the inhomogeneous structure is about the same order of magnitude as the wavelength of light, i.e., of submicron or smaller. On the other hand, for low  $\phi_0$  gels, the characteristic length may be large because the speckle pattern shows strong position dependence (Fig. 5). Therefore, it is expected that the gels prepared in high  $\phi_0$  region have dense and complicated structure in submicron scale due to the existence of many topologically entangled points as well as due to many chemically-cross-linked points in the network structure. Possible origins of such structures are discussed in detail below.

Let us take another point of view in order to answer a question how to synthesize homogeneous gels. For as-prepared gels, an intermediate concentration is preferred to make homogeneous network on submicron scales. This is due to the effect of crossover among subchains. At low concentrations, the crossover is so small that cross-linking reaction does not proceed well and prepared gels tend to have many defects in their network. At high concentrations, the extensive crossover results in many topological entanglements among subchains as well as many cross-linking points. The prepared gels tend to have many dense regions and can be characterized by a weak segregation of network. Even for equilibrium swollen gels, the intermediate concentration is preferred for the preparation of homogeneous network on submicron scales. As suggested above, the swelling to equilibrium always enlarges the submicron-scale static inhomogeneity. Therefore, gels remain homogeneous at intermediate swelling levels.

### C. The swelling-induced modulation of the dynamic fluctuation

By using SMLS, the ensemble-averaged correlation function of inhomogeneous gels can be determined correctly. From the distribution function of relaxation time,  $P_{\text{en}}(\mathbf{q}, \tau_R)$ , we can extract a good deal of information on the inhomogeneities on the scale of the mesh size of gel network, i.e., on the scale of nanometer.

The  $\phi$  dependences of  $\langle I_d(\mathbf{q}, t) \rangle_{\text{en}}$  and  $D_{\text{coop}}$  (Figs. 8 and 13) show that the ensemble-averaged values of dynamic

properties of gels depend linearly in log-log scale on the volume fraction at the time of measurement,  $\phi_0$  or  $\phi$ , regardless of the gel being in as-prepared or equilibrium-swollen state. It means that the ensemble-averaged dynamic properties are induced by thermal fluctuations. Thus, the osmotic pressure is important and it directly corresponds to the volume fraction at the time of measurement. Therefore, the ensemble-averaged dynamic properties are modulated by swelling through the  $\phi$  change from  $\phi_0$  in preparation to  $\phi$  in measurement.

Now, note again the  $\phi$  dependence of  $D_{\text{coop}}$  shown in Fig. 13. As mentioned above,  $D_{\text{coop}}$ , which is of the order of nanometers, corresponds to the mesh size of the network. Hence, it means that the mesh size of gel network is almost always controlled by the volume fraction at the time of measurement. Concerning the slope of  $D_{\text{coop}}$  versus  $\phi$ , there is a discrepancy between the present results and the blob theory [3]. It may come from the crossover behavior between dilute and semidilute solutions. There is a crossover concentration  $\phi^*$  between them. In the low  $\phi$  limit of dilute polymer solutions (not for gels), the diffusion coefficient  $D$  is equal to  $D_0$ , which corresponds to the hydrodynamic radius of isolated blobs of polymer chains. Then  $D$  begins to increase with the increase in  $\phi$  as  $D = D_0(1 + k\phi + \dots)$  even for  $\phi < \phi^*$  [26], where  $k$  is a concentration coefficient. Above  $\phi^*$ , the  $\phi$ -dependence of  $D$  becomes marked, with a slope of 3/4, which can be explained by the blob theory. It is known [27] that at  $\phi^*$  the value of slope changes from a small value to 3/4 continuously, and an intermediate value of the slope is sometimes observed around  $\phi^*$ . Therefore, for gels, such an intermediate value may be observed. Concerning the gels prepared in the present study, it is difficult to synthesize sample gels with  $\phi$  much higher than  $\phi^*$ . Thus, the actually observed slope does not reach 3/4. Further, as shown in Fig. 13, some plotted points for the lowest  $\phi$  and the highest  $\phi_0$  drop off from the power-law function. We consider that the drop off of the lowest  $\phi$  is due to defects in highly swollen gels and that of the highest  $\phi_0$  comes from some kinds of inhomogeneities in the mesh size. The latter phenomenon will be discussed below.

For the analysis of inhomogeneities, the swelling-induced change in the dispersion of  $P_{\text{en}}(\mathbf{q}, \tau_R)$  shown in Fig. 15 is noteworthy. We consider that the dispersion  $\sigma$  corresponds to the distribution width of mesh size. Thus, it directly reflects the inhomogeneities of gel network on the scale of nanometers. At low  $\phi_0$ ,  $\sigma$  increases strongly with swelling. It means some of the nanometer-size defects of gel network are enlarged by swelling. We suppose that by swelling many voids emerge in the network. On the other hand, at high  $\phi_0$ ,  $\sigma$  decreases with swelling. This is apparently anomalous behavior because it means that the nanometer-scale concentration fluctuation of the network is focused by swelling. The possible explanation of this interesting phenomenon will be discussed in the following section.

#### D. A model of inhomogeneous network structure

As mentioned above, the swelling-induced modulation is obviously different for static and dynamic fluctuations. In

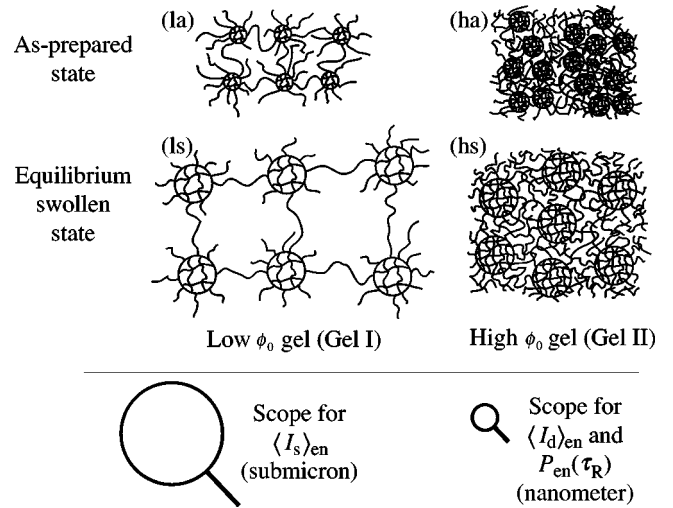


FIG. 17. Illustrations of as-prepared and equilibrium swollen network structure of the macrogels formed from microgels in low and high monomer volume fractions in preparation,  $\phi_0$ .

order to clarify this point, we note that the spatial scales of these two kinds of fluctuations observed in the present study by SMLS are different. The static fluctuations measured as  $\langle I_s(\mathbf{q}) \rangle_{\text{en}}$  correspond to the static inhomogeneities of concentration on a submicron scale. The dynamic fluctuations measured as  $\langle I_d(\mathbf{q}, t) \rangle_{\text{en}}$  and  $P_{\text{en}}(\mathbf{q}, \tau_R)$  correspond to the width of mesh-size distribution on nanometer scales. Therefore, the difference of swelling-induced modulation between dynamic and static fluctuations means that the nature of inhomogeneities on nanometer scales is essentially different from that on submicron scale. This suggests the existence of a kind of hierarchical structure in vinyl-type polymer gels.

In order to illustrate the anomalous behavior of the swelling-induced modulation, a model of network structure for vinylpolymer gels is proposed here. In the preparation of vinylpolymer gels, radical copolymerization of a monomer and a cross-linker is always performed. As the number of functional groups, e.g., vinyl groups, in the cross-linker is usually larger than that in the monomer, the reaction rate of the cross-linker is statistically larger than that of the monomer in the first stage of polymerization and many multi-branching polymer molecules, i.e., many microgels are produced. In the second stage, when the concentration of the cross-linker has decreased, the rest of the virgin monomer molecules start to react with the microgels, which grow in size and get connected with each other. In this way microgels aggregate into a macrogel. In these processes, two kinds of reactions, i.e., intramicrogel chain growth and intermicrogel connection, statistically compete depending on the concentrations of monomer, cross-linker, and microgels.

At low monomer concentrations ( $\phi_g < \phi_0 \leq \phi_c$ , i.e., gel I region shown in Fig. 2), the intramicrogel reaction may be much faster than the intermicrogel one, so that an incomplete network structure will be formed with many defects existing among the microgels. The network structure formed in this condition is illustrated in (1a) of Fig. 17. During the formation of such structure, the aggregation of microgels occurs inhomogeneously and near the gelation concentration  $\phi_g$ , a

fractal-like network structure is preferably formed from microgels as constituent components. Some of the present authors (H.F. and M.O.) tried to apply this model to the preparing-concentration dependence of viscosities of PAAm sol solutions [16].

On the other hand, at high monomer concentrations ( $\phi_c \lesssim \phi_0$ , i.e., gel II region shown in Fig. 2), the intermicrogel reaction can proceed more frequently than the intramicrogel one in the second stage of gelation, so that a dense and complex network will be formed with many topological entanglements among microgels. The network structure in this condition is shown in (ha) of Fig. 17. In the case of high monomer concentrations, microgels fill up most of the solution in preparation. The spatial distribution of microgels inevitably develops an extent of inhomogeneity, which depends on the aggregation process of microgels. Hence, microgels are separated by thin spaces of varying size filled with large number of topological entanglements, which behave like cross-linking points. Further, once the aggregation of microgels starts, it is often locally accelerated, and large-scale inhomogeneity belonging to the hierarchy of a higher rank may emerge. Concerning this phenomenon, appearance and subsequent disappearance of turbidity was observed by one of the present authors (K.H.) [15] during the cross-linked copolymerization of methyl methacrylate with ethylene dimethacrylate around 20–30% conversion. Thus, the gels prepared in high monomer concentrations tend to have much larger-scale inhomogeneity than those prepared in low monomer concentrations.

Next, based on the proposed model for as-prepared states illustrated in (la) and (ha) of Fig. 17, we try to explain the swelling-induced modulation of inhomogeneities. We start from the case of low monomer concentrations and next go to the case of high monomer concentrations.

Concerning the low-concentration gels prepared in gel I region,  $\langle I_s(\mathbf{q}) \rangle_{\text{en}}$  increases with swelling (Fig. 8). The extent of growth of  $\langle I_s(\mathbf{q}) \rangle_{\text{en}}$  due to swelling increases as the apparent swelling ratio  $\alpha$  increases. Such a behavior can be explained by the Bastide's model [9,10] discussed above. That is to say, since this network structure has a large number of defects, densely cross-linked parts swell little and sparsely cross-linked parts swell extensively. Thus, the inhomogeneity, frozen in the network structure as the distribution of cross-linking points, grows with swelling. Moreover, the mesh-size distribution  $\sigma$  broadens with swelling (Fig. 15), and the distribution becomes bimodal at the lowest concentration,  $\phi_0 = 0.026$  (Fig. 14). While the mesh size in a large part of gels enlarges with swelling, a small part of meshes may remain same in size as in the as-prepared state. That is to say, a kind of microscopic phase separation may occur with swelling. In such a case, a macroscopic volume fraction  $\phi$  calculated from the volume of the swollen gel is not equal to the microscopic local volume fraction. Actually, in low volume fractions of  $\phi \leq 0.01$ , the diffusion coefficient  $D_{\text{coop}}$  drops down from the power law of  $D_{\text{coop}}$  versus  $\phi$  (Fig. 13). Since a large portion of network meshes are swollen in a fractal manner, apparent  $D_{\text{coop}}$  becomes smaller than that calculated from  $\phi$ . We can recognize from these facts that swollen gels prepared in gel I region have very heterogeneous

structure where a small amount of dense part formed in the as-prepared microgels remains and a large amount of thin region exists among microgels, as shown in (ls) of Fig. 17.

On the other hand, concerning the high-concentration gels prepared in gel II region,  $\langle I_s(\mathbf{q}) \rangle_{\text{en}}$  for the highest concentration as-prepared gels of  $\phi_0 = 0.32$  depends on the scattering angle (Fig. 8). This suggests that there exist large-scale inhomogeneities. The autoacceleration of microgel aggregation occurring at the high monomer concentration may cause turbulence in the spatial distribution of microgels. Thus there exist locally dense and thin regions on a submicron scale, which bring about static fluctuations of the local osmotic pressure. Moreover, for high-concentration gels, the scattering angle dependence of  $\langle I_s(\mathbf{q}) \rangle_{\text{en}}$  tends to diminish with swelling (Fig. 8) and the position dependence of the scattering intensity sharpens with swelling (Fig. 5). Although it is possible to assume from these results that the characteristic length of the large-scale inhomogeneity decreases, more detailed observation should be performed in future for its confirmation. Further, concerning the dynamic fluctuation, apparent  $D_{\text{coop}}$  for the highest concentration as-prepared gels of  $\phi_0 = 0.32$  drops down from the power law of  $D_{\text{coop}}$  versus  $\phi_0$  (Fig. 13). This suggests that the acceleration of microgel aggregation occurring in the highest monomer concentration may create thin-concentration parts of the network, with large-size meshes on nanometer scales. The mesh-size distribution  $\sigma$  is forced to sharpen anomalously by swelling, and the relationship of  $\sigma$  with  $\phi_0$  shows a kind of power-law behavior (Fig. 15). From these viewpoints, we can say that high-concentration gels prepared in gel II region tend to dilute nanometer-scale inhomogeneity with swelling, as illustrated in (hs) of Fig. 17. By swelling, the microgels swell themselves and regularize their distribution to homogenize the fluctuation of the local osmotic pressure. Thus, the effective mesh sizes both inside and outside of the microgels become similar in equilibrium swollen state. Since the microgels themselves, however, play a role of effective small scatter points for static scattering, many microgels embedded in network structure may cause large static scattering intensity in high  $\mathbf{q}$  range.

Further, at intermediate monomer concentrations in preparation, around the boundary between gel I and gel II regions, i.e.,  $\phi_0 \sim \phi_c$ , the network structure of as-prepared gels may be an intermediate between (la) and (ha). Since the apparent swelling ratio  $\alpha$  shows a minimum around  $\phi_0 \sim \phi_c$  (Fig. 3), the swelling-induced modulation of fluctuations is also lowest around  $\phi_0 \sim \phi_c$ , then the least, and the network structure may be somewhat similar to (hs). The chain concentrations at the inside and outside of microgels are almost the same. Hence, there are not many defects and entanglements. Therefore, the effect of inhomogeneities on both static and dynamic properties tends to be weaker for both as-prepared and equilibrium swollen gels of  $\phi_0 \sim \phi_c$ .

In general, vinylpolymer gels are synthesized in a two-stage process, where in the first stage many microgels are produced and in the second stage a macrogel is formed from the microgels. Therefore, it can be said that usual vinylpolymer gels are essentially inhomogeneous. In order to prepare homogeneous structure of a gel network, alternative prepara-

tion methods must be considered. From this viewpoint, some of the present authors (H.F. and K.H.) have studied the gelation of main-chain aromatic polyimides under polycondensation reactions [28]. We can consider that in contrast to vinylpolymer systems, the gelation process in such a system proceeds according to a percolation model. The SMLS study of polyimide gels will be reported elsewhere.

## VI. CONCLUSION

The static and dynamic fluctuations in inhomogeneous vinylpolymer gels have been studied. By using SMLS and a formula for inhomogeneous media, the ensemble-averaged

properties were determined. Especially, ensemble-averaged relaxation-time distribution  $P_{en}(\mathbf{q}, \tau_R)$  was determined rigorously. It enabled us to study in detail a mesh-size distribution of network structure in polymer gels. Considering experimental results, differences between two types of gels, prepared at low and high total monomer concentrations, with respect to the swelling-induced modulation of the static and dynamic fluctuations were discussed. In order to explain the differences in modulation behavior, a model of network structure was introduced. It was proposed that vinylpolymer macrogels are usually formed by connecting many pre-formed microgels.

- 
- [1] E. Geissler, in *Dynamic Light Scattering*, edited by W. Brown (Clarendon Press, Oxford, 1993), Chap. 11.
- [2] T. Tanaka, L. Hocker, and G.B. Benedek, *J. Chem. Phys.* **59**, 5151 (1973).
- [3] P.G. de Gennes, *Scaling Concepts in Polymer Physics* (Cornell University Press, Ithaca, New York, 1979).
- [4] P.N. Pusey and W. van Megen, *Physica A* **157**, 705 (1989).
- [5] J.G.H. Joosten, E.T.F. Geladé, and P.N. Pusey, *Phys. Rev. A* **42**, 2161 (1990).
- [6] J.G.H. Joosten, J.L. McCarthy, and P.N. Pusey, *Macromolecules* **24**, 6690 (1991).
- [7] H. Furukawa and S. Hirotsu, *J. Phys. Soc. Jpn.* **71**, 2873 (2002).
- [8] M. Shibayama, *Macromol. Chem. Phys.* **199**, 1 (1998), and references therein.
- [9] J. Bastide and L. Leibler, *Macromolecules* **21**, 2649 (1988).
- [10] J. Bastide, L. Leibler, and J. Prost, *Macromolecules* **23**, 1821 (1990).
- [11] A. Onuki, *Adv. Polym. Sci.* **109**, 63 (1993).
- [12] P.J. Flory, *Principles of Polymer Chemistry* (Cornell University Press, Ithaca, NY, 1953).
- [13] D. Stauffer, *Introduction to Percolation Theory* (Taylor & Francis, London, 1985).
- [14] K. Dušek, *Development in Polymerization 3. Network Formation and Cyclization in Polymer Reactions* (Applied Science Publishers, London, 1982), Chap. 4.
- [15] K. Horie, A. Otagawa, M. Muraoka, and I. Mita, *J. Polym. Sci., Polym. Chem. Ed.* **13**, 445 (1975).
- [16] D. Katayama, H. Furukawa, and M. Okada, *Trans. Mater. Res. Soc. Jpn.* **25**, 775 (2000).
- [17] H. Furukawa, *J. Mol. Struct.* **554**, 11 (2000).
- [18] H. Furukawa and M. Okada, *Trans. Mater. Res. Soc. Jpn.* **25**, 723 (2000).
- [19] B.J. Berne and R. Pecora, *Dynamic Light Scattering* (Wiley, New York, 1976).
- [20] R. Loudon, *The Quantum Theory of Light*, 3rd ed. (Oxford University Press, Oxford, 2001).
- [21] E. Geissler, F. Horkay, and A.-M. Hecht, *J. Chem. Phys.* **102**, 9129 (1995).
- [22] K. Ema and H. Yao, *Solid State Phys.* **29**, 677 (1994).
- [23] K. Ohbayashi, S. Kagoshima, and A. Ikushima, *Solid State Phys.* **7**, 22 (1972).
- [24] J.G. McWhirter and E.R. Pike, *J. Phys. A* **11**, 1729 (1978).
- [25] N. Ostrowsky, D. Sornette, P. Parker, and E.R. Pike, *Opt. Acta* **28**, 1059 (1981).
- [26] W. Brown and T. Nicolai, in *Dynamic Light Scattering*, edited by W. Brown (Clarendon Press, Oxford, 1993), Chap. 6.
- [27] I. Teraoka, *Polymer Solutions* (Wiley, New York, 2002).
- [28] J. He, S. Machida, H. Kishi, K. Horie, H. Furukawa, and R. Yokota, *J. Polym. Sci., Part A: Polym. Chem.* **40**, 2501 (2002).